Materials Advances

ROYAL SOCIETY OF CHEMISTRY

PAPER

View Article Online
View Journal | View Issue

Check for updates

Cite this: *Mater. Adv.*, 2025, 6, 4220

Ionic liquid modified mesoporous silica nanocarriers for efficient drug delivery and hydrophobic surface engineering†

Annika Szymura,‡ Shaista Ilyas, *‡ Florian Grohmann and Sanjay Mathur

Attaining covalent attachment of diverse molecules onto carrier surfaces without compromising their chemical identity and biological functionality remains a challenge. Here, a newly synthesized alkyne-functionalized ionic liquid, 1-hexadecyl-3-propargyl imidazolium bromide (HDPI), was chemically attached on the surface of azide-modified mesoporous silica nanocarriers ($mSiO_2$, av. size 110 nm) based on the Menshutkin reaction and copper-catalyzed click chemistry. The HDPI-functionalized $mSiO_2$ nanocarriers were loaded with tetracycline (TC) to develop a dual-action drug delivery system. Time-dependent drug release studies conducted at pH 7.4 and 37 °C over 48 h revealed controlled TC release. The long alkyl chain of the surface-bound ionic liquids (ILs) facilitated bacterial cell wall penetration, enhancing TC transport into both Gram-positive and Gram-negative bacteria. This dual-action mechanism was validated through antibacterial assays demonstrating that the surfactant-like IL disrupts bacterial cytoplasmic membranes, while the antibiotic induces cell death. Given the inherent antibacterial properties of ILs, we further investigated their ability to form stable, hydrophobic, and antimicrobial coatings on glass substrates under different environmental conditions. The results indicate that these IL-based coatings are uniform, durable, and hold significant potential for applications in healthcare and industry.

Received 18th December 2024,
Accepted 9th April 2025

DOI: 10.1039/d4ma01267d

rsc.li/materials-advances

Open Access Article. Published on 15 May 2025. Downloaded on 4/16/2026 5:58:42 PM.
This article is licensed under a Creative Commons Attribution 3.0 Unported Licence.

Introduction

The rise of multi-drug resistant pathogens in the human environment poses a serious threat to human health. The excessive misuse and overuse of conventional antibiotics in the food industry, health care, clinical settings, agriculture, and aquaculture have accelerated the development of drug-resistant pathogens, rendering many established chemotherapeutics and treatments ineffective.[1] Consequently, effective treatment options may be exhausted by 2050, leading to life-threatening infections, if the development of new anti-infectives slows down. To combat the growing threat of antibiotic resistance to health, new compounds and strategies targeting novel molecular pathways are being developed.[2,3] Unlike traditional antibiotics, which act on intracellular targets while preserving bacterial morphology, surface-active ionic liquids (SAILs), quaternary ammonium compounds (QUACs), and antimicrobial peptides (AMPs) physically disrupt bacterial membranes making resistance development challenging.[4–7] Although bacteria can rapidly evolve defense mechanisms against conventional antibiotics, effective resistance to amphiphilic agents is rare, as it requires substantial remodeling of membrane lipid composition.[8,9]

Imidazolium-based ionic liquids exhibit inherent antimicrobial properties, primarily resulting from their alkyl chain optimally constituted by 12 to 16 carbon atoms.[8–11] These long-chain compounds can self-assemble into micellar structures in the liquid phase, disrupting bacterial cytoplasmic membranes through hydrophobic interactions. The antibacterial activity mechanism of surface-active ionic liquids (SAILs) closely resembles that of positively charged quaternary ammonium compounds (QUACs).[12–14]

Different strategies have been explored to fortify the antibacterial efficacy of existing biocides, including structural modifications and innovative delivery systems.[15–17] Another approach involves developing new antimicrobial agents based on combinations of biocidal molecules in traditional or neoteric formulations.[18,19] For example, Deng *et al.* demonstrated that loading different antibiotics (*e.g.*, enoxacin, kanamycin, neomycin, tetracycline, *etc.*) onto silver nanoparticles resulted

Institute of Inorganic and Materials Chemistry, University of Cologne, Greinstr. 6, 50939, Cologne, Germany. E-mail: silyas@uni-koeln.de

† Electronic supplementary information (ESI) available: ^{1}H-NMR spectrum of HDI (DMSO-d_6, 300.1 MHz). ^{13}C-NMR spectrum of HDI (DMSO-d_6, 75.7 MHz). ^{1}H-NMR spectrum of HDPI (DMSO-d_6, 300.1 MHz). ^{13}C-NMR spectrum of HDPI (DMSO-d_6, 75.7 MHz). Absorption spectra and relevant calibration curve of pure solution of tetracycline. Release efficiency (%) of bare and HDPI-conjugated mesoporous silica nanocarriers. See DOI: https://doi.org/10.1039/d4ma01267d

‡ Annika Szymura and Shaista Ilyas contributed equally as primary authors to this manuscript.

© 2025 The Author(s). Published by the Royal Society of Chemistry

Open Access Article. Published on 15 May 2025. Downloaded on 4/16/2026 5:58:42 PM. This article is licensed under a Creative Commons Attribution 3.0 Unported Licence.

in synergistic bacteriostatic effects against drug-resistant bacteria *S. enterica*.[20] Similarly, B. F. Gilmore *et al.* linked 1-hexadecyl imidazolium derivatives encompassing alkyl chain length from C_8 to C_{18} with metal ion-containing anions ($[AgBr_2]^-$ and $[CuCl_4]^-$) to enhance toxicity against various Gram-positive and Gram-negative pathogens, and fungi.[21] Moreover, Z. Zheng *et al.*, assessed polyionic liquid (PIL) membranes coordinated with metallic anions ($ZnCl_2$, $CuCl_2$, and $FeCl_3$) for their bactericidal effects against *E. coli* and *S. aureus*.[22] Additionally, Lebedeva *et al.* investigated polymer ionic liquids as a greener alternative to conventional antibacterial agents in medical applications.[23] Likewise, Mathur *et al.* have reported the use of green tea derivatives as water-soluble and biocompatible surface active ligands and clickable imidazolium-based C16 ionic liquids with a surfactant-like structure bound to the surface of magnetic iron oxide nanoparticles with high antibacterial activity against various bacterial strains and selective uptake of heavy metals and organic pollutants from wastewater.[12,24]

D. D. Yang *et al.* evaluated the combination of 1-hexadecyl imidazolium derivatives with long alkyl chains and organic anions of traditional antibiotic molecules (*e.g.*, ampicillin, penicillin G, amoxicillin, tetracycline, and doxycycline) to create novel active pharmaceutical ingredient-ionic liquids (API-ILs). These formulations exhibited enhanced toxicity towards various Gram-positive and Gram-negative bacteria including drug-resistant strains (*e.g.*, *S. aureus, methicillin-resistant S. aureus* (MRSA), *E. coli*, *K. pneumoniae, etc.*).[20,23–26]

This study explores the potential of clickable HDPI-based ionic liquids on $mSiO_2$ and glass surfaces for controlled drug release and the development of antibacterial, hydrophobic coatings.

Results and discussion

Synthesis and characterization of 1-hexadecyl-3-propargyl imidazolium bromide

HDPI, a new imidazole-based ionic liquid derivative, was synthesized following the Menshutkin reaction, an S_N2 nucleophilic substitution reaction. This reaction converts a tertiary amine to a quaternary ammonium salt by reaction with an alkyl halide alkylating agent (Scheme 1).

In a two-step chemical approach, initially, 1-hexadecyl imidazole (HDI) was first prepared by a nucleophilic substitution reaction under inert reaction conditions.[28] A nucleophilic substitution reaction was carried out between the starting materials imidazole and 1-bromo hexadecane after the nitrogen atom of the imidazole core was activated by deprotonation with a base (KOH). After purification of the pale-yellow solid intermediate, HDI was used to interact with propargyl bromide to generate the desired HDPI derivative (Scheme 1).[29] Afterwards, the nucleophilic substitution reaction, a white solid product precipitated from the toluene reaction mixture upon the slow addition of water. The product was then purified and dried, resulting in a yield of 74.6%.

To evaluate the synthesis of HDPI, ^{1}H NMR and ^{13}C NMR studies were conducted (Fig. 1 and Fig. S1, ESI†). Because the 1-hexadecyl imidazolium bromide derivative consists of a positively charged imidazolium core and a long hydrophobic C_{16} alkyl chain, the chemical shifts of the protons and carbon atoms for the imidazolium core as well as for the hydrocarbon chain are evident in the ^{1}H NMR and ^{13}C NMR spectra of HDPI. The ''carbene''-like C-5 atoms of HDPI show a shielded character (136.06 ppm) due to the electron-rich propargyl group attached to the adjacent nitrogen atom, which can enter into conjugation with the aromatic imidazolium core. The signals of chemical shifts for the protons and carbon atoms are displayed at 5.22 (H-22) and 3.85 (H-24) ppm, respectively. Because the 1-hexadecyl imidazolium bromide derivative is hygroscopic, residues of water were detected in the recorded ^{1}H NMR spectra (peak around 3.33 ppm).[12] The as-synthesized HDPI was further characterized by FT-IR spectroscopy (Fig. 1(C) and Fig. S3, ESI†). The prominent bands at 2914 and 2852 cm^{-1} correspond to the alkyl C–H stretching vibrations of the C_{16} hydrocarbon long chain and the peak at 1166 cm^{-1} belongs to the C–H deformation vibration.

The signals appearing at 1563 and 1469 cm^{-1} belong to the ring stretching vibrations of the skeleton of the imidazolium core (C═C and C═N). In addition, the distinct absorption peaks between 870 and 605 cm^{-1} can also be assigned to C–N stretching vibrations of the imidazole. The signals at 2120 and 3155 cm^{-1} can be referred to the stretching vibrations of –C≡C– and –C≡C–H of the propargyl group of HDPI.[12,30] The table in D displays the *m*/*z* values for the molecular peaks detected at their highest intensities for the 1-hexadecyl imidazolium derivative by electrospray ionization mass spectrometry (Fig. 1 and Fig. S1 and 2, ESI†). Since ESI-MS is a mild ionization method with negligible molecular fragmentation, the obtained *m*/*z* values correspond to the molecular weight of the positively charged ionic liquid molecules. These molecules feature an imidazolium core with the conjugated functional group and a hydrophobic alkyl excluding the counterion bromide.[12]

Mesoporous silica ($mSiO_2$) nanocarriers with an average size of 110 nm ± 3 nm were synthesized using CTAB molecules as a

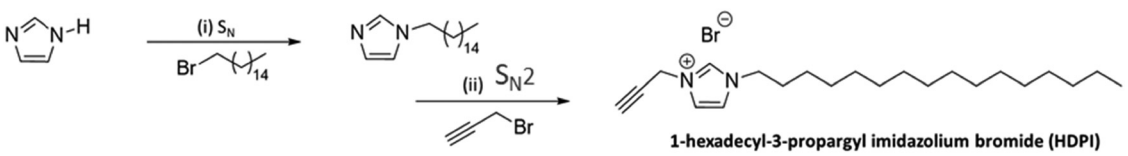

Scheme 1 Synthetic pathway for the 1-hexadecyl imidazolium bromide derivative, 1-hecxadecyl-3-propargyl imidazolium bromide, prepared by conducting the Menshutkin reaction under following conditions: (i) DMSO, KOH, N_2, 6 h, and 70 °C, (ii) toluene, 24 h, and 110 °C.[27–29]

Open Access Article. Published on 15 May 2025. Downloaded on 4/16/2026 5:58:42 PM.
This article is licensed under a Creative Commons Attribution 3.0 Unported Licence.

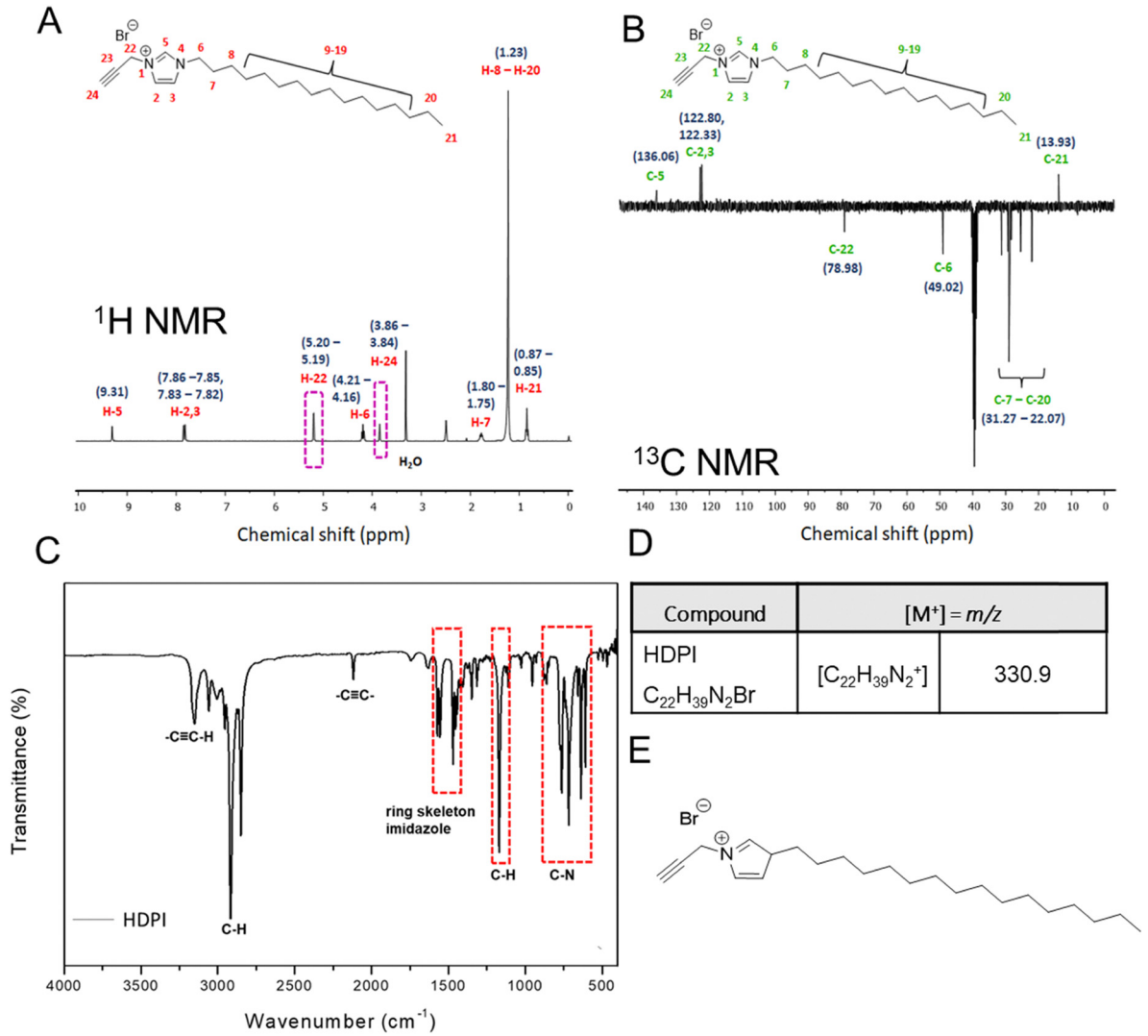

Fig. 1 (A) and (B) ^{1}H NMR and ^{13}C{^{1}H} DEPTQ (135) NMR spectra of HDPI recorded in DMSO-d_6 and interpretation of assigned chemical shifts (δ in ppm, blue numbers) to proton and carbon atoms of the compound (red and green numbers, respectively). The pink dashed box labels the signal of the propargyl group, connected to the nitrogen atom of the imidazolium core (C) FT-IR spectra of HDPI labeled with most prominent vibration bands. (D) Table shows *m/z* values for the molecular peaks with highest intensities detected of HDPI recorded *via* ESI-MS. The table also depicts the positively charged molecular fragments of the as-prepared IL attributed to the measured *m/z* values. (E) Chemical structure of HDPI.

soft template. To explore potential synergy in this approach, the antibiotic tetracycline was loaded into mesoporous silica nanocarriers, while HDPI was covalently bonded on the surface of $mSiO_2$ using the copper catalyzed click reaction (Scheme 2).

Initially, silanization with bromo-silane resulted in Br-$mSiO_2$, which was subsequently converted to N_3-$mSiO_2$ nanocarriers *via* an (S_N2) nucleophilic substitution reaction. The alkyne-functionalized HDPI was then conjugated to N_3-$mSiO_2$ using a copper-catalyzed azide–alkyne cycloaddition reaction (CuAAC), resulting in HDPI-$mSiO_2$ nanocarriers. Following this conjugation, the nanocarriers were loaded with tetracycline (TC), and time-dependent drug release studies were conducted to evaluate the release kinetics. The binding of HDPI *via* click chemistry protocols operates under mild conditions, making it ideal for preserving the structure of both the ionic liquid and the mesoporous silica. Its efficiency and selectivity ensure a strong, stable bond, reducing the risk of leaching and improving long-term performance.[32–34] The antibacterial activity of the HDPI-conjugated, TC-loaded nanocarriers was tested against both Gram-positive (*E. coli*) and Gram-negative (*B. subtilis*) bacterial strains.

Surface composition analysis of HDPI-conjugated mesoporous nanocarriers

Fig. 2 shows the recorded FT-IR spectra of the bare $mSiO_2$ and stepwise surface HDPI-functionalized nanocarriers. The existence of silica is accompanied by the absorption peaks at 1077, 798 and 449 cm^{-1}, associated with asymmetric and symmetric stretching and bending modes of Si–O–Si. The broad vibration band around 3321 cm^{-1} and the band at 958 cm^{-1} are typically attributed to the rich presence of silanol groups (Si–OH) on the surface of bare $mSiO_2$. Moreover, weak peaks at 2928 and

© 2025 The Author(s). Published by the Royal Society of Chemistry

Open Access Article. Published on 15 May 2025. Downloaded on 4/16/2026 5:58:42 PM.
This article is licensed under a Creative Commons Attribution 3.0 Unported Licence.

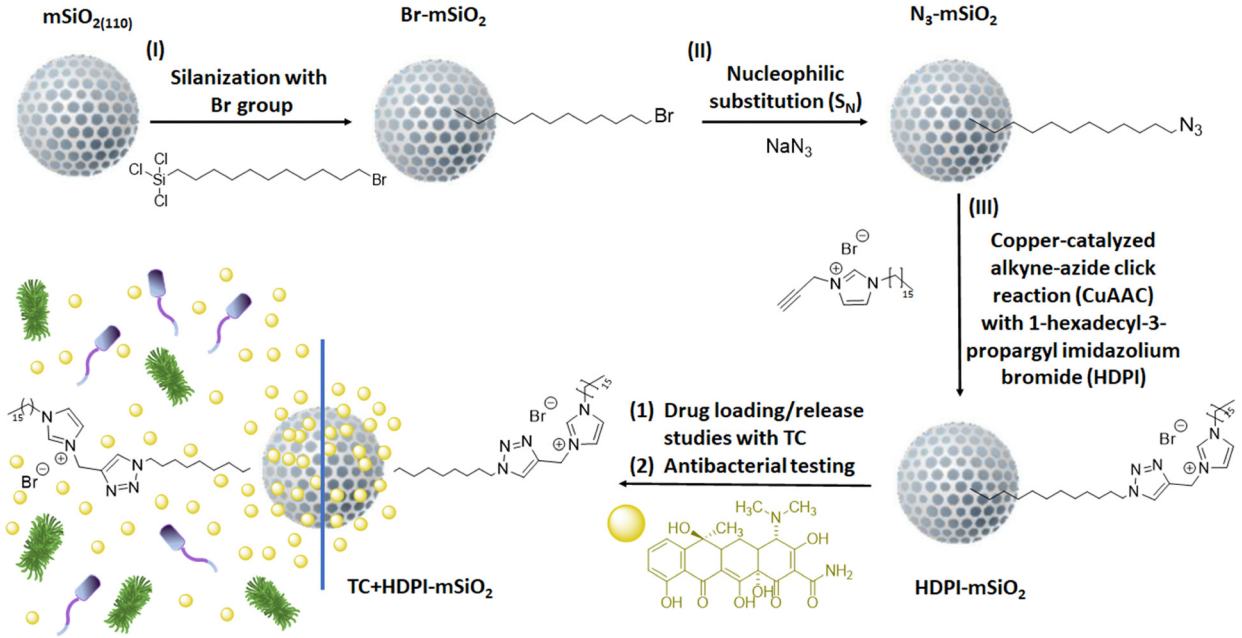

Scheme 2 Schematic pathway for the design and synthesis of the HDPI-$mSiO_2$ carriers as antibacterial drug conjugates. The HDPI- functionalized $mSiO_2$ nanocarriers were loaded with tetracycline following a time-dependent tetracycline release profile at ambient temperature. Additionally, their concentration-dependent antibacterial activity was evaluated against Gram-positive and Gram-negative bacteria (*E. coli* and *B. subtilis*). Tetracycline exhibits bactericidal activity against a wide range of Gram-positive and Gram-negative bacteria. Its mode of action is based on the inhibition of protein synthesis in the bacterial cell (inhibition of translation through interaction with the ribosome 30S subunit of the ribosome).[31]

2848 cm^{-1} are assigned to the symmetric and asymmetric stretching vibrations of C–H groups belonging to the alkyl chains of the residual template (CTAB) used during the synthesis of particles.[30,35,36] The binding of bromo silane comprises a C_{11} hydrocarbon chain *via* a subsequent hydrolysis-condensation reaction. It leads to a further increase in intensity and a slight shift in the symmetric and asymmetric stretching vibrations of the C–H groups, as evidenced by the presence of peaks at 2924 and 2853 cm^{-1}. The exchange of bromide with an azide group in a nucleophilic substitution reaction shows no shift and change in the intensity of the C–H vibrational bands due to a simple substitution of the functional group at the end of the alkyl chain. However, a new peak at 2099 cm^{-1} corresponds to the stretching mode of the $-N_3$ group, indicating the effective substitution of the essential intermediate for the CuAAC reaction. The disappearance of the vibrational band of the azide group in the spectrum of the HDPI-conjugated $mSiO_2$ and the appearance of new peaks at 1678 and 1367 cm^{-1} can be attributed to the formation of a 1,2,3-triazole ring, which in turn reveals the covalent binding of HDPI *via* the CuAAC reaction.[30,35,36] Moreover, the presence of vibration bands at 1558 and 1468 cm^{-1} can be attributed to the ring stretching vibrations of the skeleton of the imidazolium core (C=C and C=N), while the peaks at 3127, 3101, and 3071 cm^{-1} can be assigned to the aromatic C–H stretching vibration of the imidazole ring, respectively.[12,33,37] Hence, a distinct increase in intensity and the slight shift in the symmetric and asymmetric stretching vibrations of C–H groups (2921 and 2848 cm^{-1}) can therefore be explained by the binding of HDPI comprising a long C_{16} alkyl chain to the surface of N_3-$mSiO_2$.[12,30] Zeta potential measurements were conducted at pH 7 and the surface charge showed a visible change after each chemical reaction on the surface of silica nanocarriers (Fig. 2, Table G). Bare $mSiO_2$ displayed a ζ-value of −27.7 mV due to its deprotonated silanol groups ($-Si-O^-$) on the surface. After binding bromo silane, the ζ-value decreased to −48.4 mV due to the high electron density of the bromide atom. Removal of hydroxyl surface groups by bromide anions could potentially increase the zeta potential in the more negative range. Typically, surface-hydroxyl groups contribute to surface charge through the deprotonation of hydroxyl groups at basic pH. The replacement of hydroxyl (–OH) groups by bromide anions (Br^-), which do not participate in hydrogen bonding, leads to more effective negative surface charge, leading to an increase in the zeta potential in the negative direction. Replacement of the bromo to an azide group in a nucleophilic substitution reaction led to a slight increase in the ζ-value to −44.8 mV. A dominant shift to positive values (+25.1 mV) is observed after the click conjugation of HDPI due to the attachment of the positively charged imidazolium core.[30,38,39] It can be observed that with the increasing density of ligands or molecules bound to the surface of $mSiO_2$, the carbon and hydrogen contents increase accordingly, which is reflected in the increasing values of C(%) and H(%). Following the nucleophilic substitution reaction, a nitrogen content of (N(%) = 0.10) was observed, indicating the introduction of the azide group onto the nanocarriers. After the click reaction, the nitrogen content was found to increase (N(%) = 0.42), confirming the presence of additional ligands on

Open Access Article. Published on 15 May 2025. Downloaded on 4/16/2026 5:58:42 PM.
This article is licensed under a Creative Commons Attribution 3.0 Unported Licence.

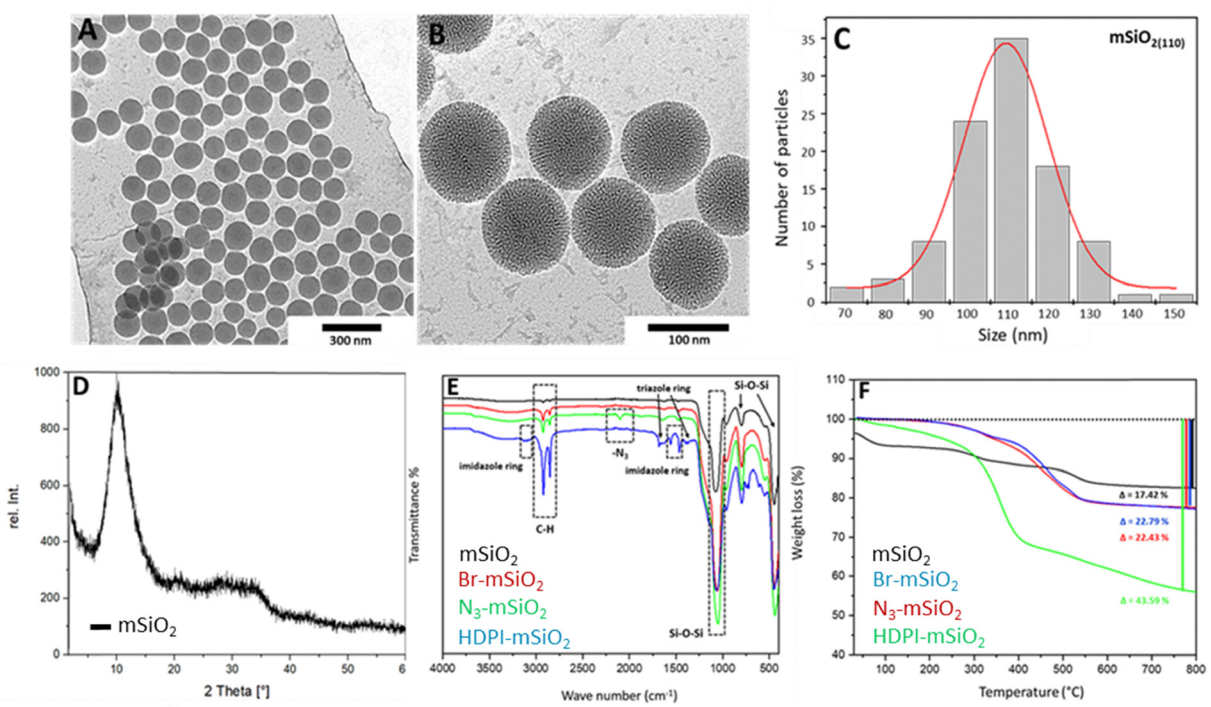

G

Sample	C (%)	H (%)	N (%)	Zeta potential ζ (mV)
$mSiO_2$	1.55	6.87	-	- 27.7 (± 0.29)
Br-$mSiO_2$	2.15	10.50	-	- 48.4 (± 0.64)
N_3-$mSiO_2$	2.13	10.41	0.10	- 44.8 (± 0.32)
HDPI-$mSiO_2$	2.46	14.32	0.42	+ 25.1 (± 0.45)

Fig. 2 (A) Transmission electron microscope (TEM) image shows the homogeneous distribution of spherical mesoporous silica particles. (B) Higher resolution TEM image confirms the existence of the porous structure of the particles. (C) Histogram of $mSiO_2$ shows an average size of 110 nm. (D) XRD diffractogram indicates the existence of an amorphous phase of nanocarriers. (E) FT-IR spectra for the bare and surface functionalized $mSiO_2$ nanocarriers reveal the change in surface chemistry upon functionalization. The absorption bands are labeled for the dominant peaks after condensation (red), nucleophilic substitution (green) and click reaction (blue) on $mSiO_2$ nanocarriers (black). (F) Thermogravimetric analysis (TGA) of bare and functionalized nanocarriers. Table (G) Elemental analysis and zeta potential analysis after each conjugation on mesoporous silica particles (in triplicate for the bare and modified $mSiO_2$ carriers).

the carries. DLS analysis showed that bare $mSiO_2$ exhibited an average hydrodynamic radius of 121 nm ± 5 nm (PDI of 0.020), leading to 143 nm ± 4 nm (PDI 0.082) after condensation and nucleophilic substitution reactions. Hydrophobic interactions increased the hydrodynamic radius to HDPI-functionalized nanocarriers in polar dispersions with an average size of 651 nm (PDI 0.475). However, the mesoporous structure remains intact, maintaining its porosity (3–4 nm) and better drug release by improving surface interactions and diffusion routes as demonstrated in our various studies.[40,41] The TGA analysis shown in Fig. 2(F) shows that in the case of Br-$mSiO_2$ and N_3-$mSiO_2$ nanocarriers, the weight loss remains nearly the same (Δ = 22.79 and 22.43% respectively), indicating that the bromide group was simply replaced by an azide group without significant changes in the overall surface modification. The highest weight loss was observed for the HDPI-conjugated $mSiO_2$ nanocarriers (Δ = 43.59%), suggesting the removal of a larger HDPI ligand and a greater degree of functionalization.[42]

Drug loading and release studies for TC-loaded HDPI-conjugated $mSiO_2$ carriers

The HDPI-conjugated $mSiO_2$ and bare $mSiO_2$ nanocarriers were loaded with TC, and time-dependent continuous release kinetics and loading capacity were evaluated at pH 7.4 and 37 °C (Fig. 3). The release of the drug was monitored by UV-Vis spectroscopy by recording absorption maximum (λ_{max}) of tetracycline (270 nm). The release efficiency RE (%) and loading capacities (LC) of bare and HDPI-conjugated $mSiO_2$ nanocarriers were calculated as follows:[39,43]

$$\mathrm{LC} = \frac{(\text{Total amount of TC} - \text{Free TC})}{\text{Nanoparticles weight}}$$

$$\mathrm{RE}\ (\%) = \frac{(\text{Total amount of TC} - \text{Free TC})}{\text{Total amount of TC}} \times 100\%$$

LC describes the amount of TC loaded into the carriers (mg TC per mg carriers). It was determined by measuring the

© 2025 The Author(s). Published by the Royal Society of Chemistry

Open Access Article. Published on 15 May 2025. Downloaded on 4/16/2026 5:58:42 PM.
This article is licensed under a Creative Commons Attribution 3.0 Unported Licence.

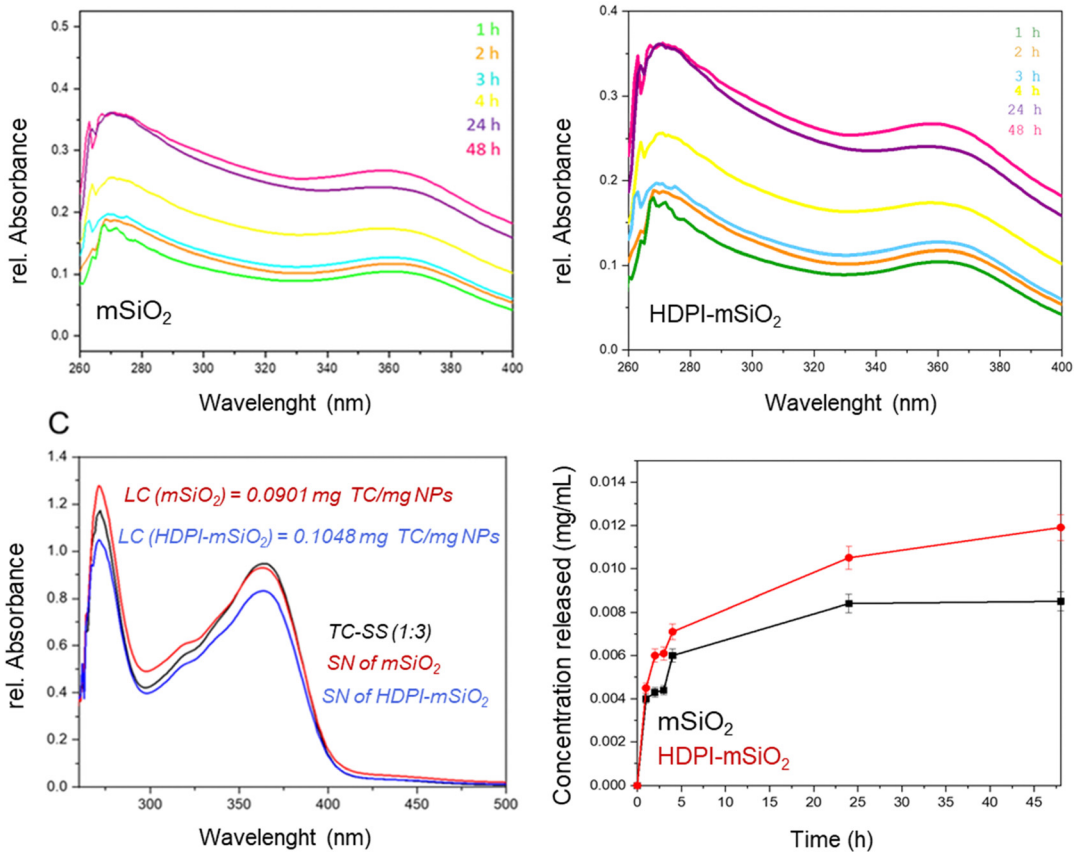

Fig. 3 Time-dependent UV-vis measurements to determine TC concentration (absorption maximum: 270 nm): (A) the bare $mSiO_2$ nanocarriers and (B) the HDPI-conjugated $mSiO_2$ separated from their supernatants after centrifugal separation at pH 7.4 (PBS buffer) and 37 °C. (C) UV-Vis spectra recorded for the TC stock solution (SS) and the supernatants (SN) after TC loading onto bare and HDPI-conjugated $mSiO_2$ nanocarriers along with the calculated LC. (D) TC concentration released at pH 7.4 (PBS buffer) and 37 °C over a 48 hour time period.

concentration of TC in the supernatants of the loaded bare and HDPI-conjugated $mSiO_2$ in comparison to the concentration of the TC stock solution (Fig. 3(C)). In contrast, RE (%) is the amount of TC released into the buffer solution per given time point (mg TC per mL buffer) relative to the amount of TC loaded into the NPs or their LC set to 100%.

HDPI-conjugated $mSiO_2$ particles showed a loading capacity of 0.1048 mg (TC per mg), while bare $mSiO_2$ demonstrated a LC of 0.0901 mg (TC per mg). These calculated values correspond to 75.0% and 77.7% in comparison to the amount of TC in the loading volume of the stock solution (0.133 mg TC per mL EtOH). The moderately higher LC of HDPI-conjugated $mSiO_2$ can be attributed to the potential of the surface conjugation chemistry and the hydrophobic long alkyl chain of HDPI. It can also be due to the aromatic π–π stacking, electrostatic interactions (aromatic positive charged imidazolium core, aromatic 1,2,3-triazole ring) and hydrogen bonds with a hydrophilic structure of TC which encompasses four aromatic rings and some smaller hydrophobic as well as a huge number of polar domains.

To validate HDPI-$mSiO_2$ nanocarriers as a drug delivery probe, time-dependent release profiles of bare and HDPI-conjugated carriers were calculated (Fig. 3(A) and (B)). Initially, in the first 6 hours, both nanocarriers showed a moderate burst release of TC followed by a controlled and sustained release kinetics of the antibiotic. After 48 hours, the total release of TC from HDPI-conjugated $mSiO_2$ nanocarriers reached 11.9 μg TC per mL buffer (2.3%) compared to 8.5 μg TC per mL buffer (3.4%) from the bare nanocarriers. After 48 hours, no more drug leached out of these carriers. These findings suggest that HDPI functionalization on nanocarriers led to a moderately higher release rate potentially due to alterations in surface interactions or drug-nanocarrier affinity. Moreover, it can be observed that only a small amount of TC is released per hour, suggesting that HDPI-$mSiO_2$ carriers can serve as beneficial drug delivery probes which could maintain effective levels of the released antibiotic at the target side for extended time periods. Finally, the initial rapid release of TC from HDPI-conjugated $mSiO_2$ carriers could provide an "antibacterial shock effect" in the beginning followed by a long-term action on pathogenic bacteria.

Antibacterial evaluation

The synergistic effect refers to the interaction of tetracycline and ionic liquids with cells producing a combined effect that is greater than the sum of their individual effects. To determine a

Open Access Article. Published on 15 May 2025. Downloaded on 4/16/2026 5:58:42 PM.
This article is licensed under a Creative Commons Attribution 3.0 Unported Licence.

potential synergistic antibacterial effect of TC-loaded HDPI-conjugated $mSiO_2$ nanocarriers, an INT violet viability assay was conducted using two different bacterial strains *B. subtilis* (Gram-positive bacterium) and *E. coli* (Gram-negative bacterium). The different concentrations of nanocarriers were dispersed in H_2O/DMSO (10 : 1) and inoculated in the bacterial cultures. The bacterial survival rates were monitored after 6 hours of incubation at 37 °C. As a negative control, the bare mesoporous silica and solvent (H_2O/DMSO (10 : 1) were utilized. As a positive control, the pure solutions of HDPI and TC (using four different concentrations) were tested in both bacterial cultures. The HDPI-conjugated $mSiO_2$ and TC + HDPI-$mSiO_2$ were evaluated for their antimicrobial activity using four different concentrations ranging from 6.25 μg mL^{-1}, 12.50 μg mL^{-1}, 25.0 μg mL^{-1} and 50.0 μg mL^{-1}).

The bare $mSiO_2$ nanocarriers in all concentrations tested showed no antibacterial activity as expected; however, the pure solutions of HDPI and TC exhibited substantial toxicity against *E. coli* (Fig. 4(A) and (B)). The result of pure TC on bacterial density was marginally higher than pure HDPI which is consistent with the fact that TC directly inhibits bacterial growth. When tested the HDPI-conjugated $mSiO_2$ nanocarriers, the lower concentration (6.25 and 12.50 μg mL^{-1}) exhibited very less antibacterial activity; however, the higher concentration (25.0 and and 50.0 μg mL^{-1}) revealed significant activity similar to pure HDPI and/or pure TC. To investigate if the dual-nanocarrier approach contributes to enhance the cell toxicity, the TC-loaded HDPI-functionalized $mSiO_2$ carriers were incubated with *E. coli* and *B. subtilis* cells (Fig. 4(A) and (B)). Importantly, the highest toxicity level of TC-loaded HDPI-functionalized $mSiO_2$ was observed with higher concentration *i.e.*, 25.0 μg mL^{-1} and 50.0 μg mL^{-1}, which is nearly similar to HDPI-$mSiO_2$, pure solution of TC, and HDPI. Interestingly, the lower concentration of TC-loaded HDPI-conjugated $mSiO_2$ (6.25 μg mL^{-1}, 12.50 μg mL^{-1}) demonstrated double of the cell toxicity when compared to HDPI-$mSiO_2$ which shows slight antimicrobial activity. Overall, these data demonstrate that the highest toxicity of functional nanocarriers against *E. coli* and *B. subtilis* confirmed the proposed potential of the enhanced effect due to the combination of both antimicrobial agents on a single nanocarrier. This shows that the dual nanocarrier approach boosts antimicrobial activity, which ultimately allows the multiple combinations of different antibiotics. In addition, the use of smaller concentration of drug molecules is always a desired method.

In our previous work, we have conducted extensive studies on mammalian cells including immune cells to evaluate the biocompatibility of bare silica and surface-modified nanocarriers and the results show that these modifications benefit to reduce toxicity and improve cell compatibility.[32,40] By evaluating cytotoxicity, cellular uptake and overall safety, our published data confirmed that surface-modified nanocarriers have greater potential for therapeutic use, further supporting their safe integration into the field of medicine.[12,30,32,40,41,44]

In the second part of the study, the potential of HDPI for producing hydrophobic and antibacterial coatings on smooth glass substrates was investigated (Scheme 3). To synthesize the coating material, alkyne-functional HDPI was effectively clicked with azide-modified PAA molecules (HDPI-PAA) and applied on the glass substrate using the drop casting approach. The resulting HDPI-functionalized PAA coatings were homogenous and stable (Fig. 5(C)). Furthermore, the stability and durability of HDPI-PAA-coated silica (glass) surfaces have been rigorously assessed under different acidic conditions, demonstrating their resistance against natural rains and varying pH levels (Scheme 3 and Fig. 5(C)). The antibacterial data in Fig. 4 confirm that HDPI molecules themselves exhibit promising antibacterial properties to make them suitable for a range of applications where microbial resistance is essential.

The FT-IR spectrum in Fig. 5(A) (red) shows click-functionalized PAA with the imidazole ring at 3130 cm^{-1}, the smaller azide band at 2100 cm^{-1} as well as the formation of the triazole ring at

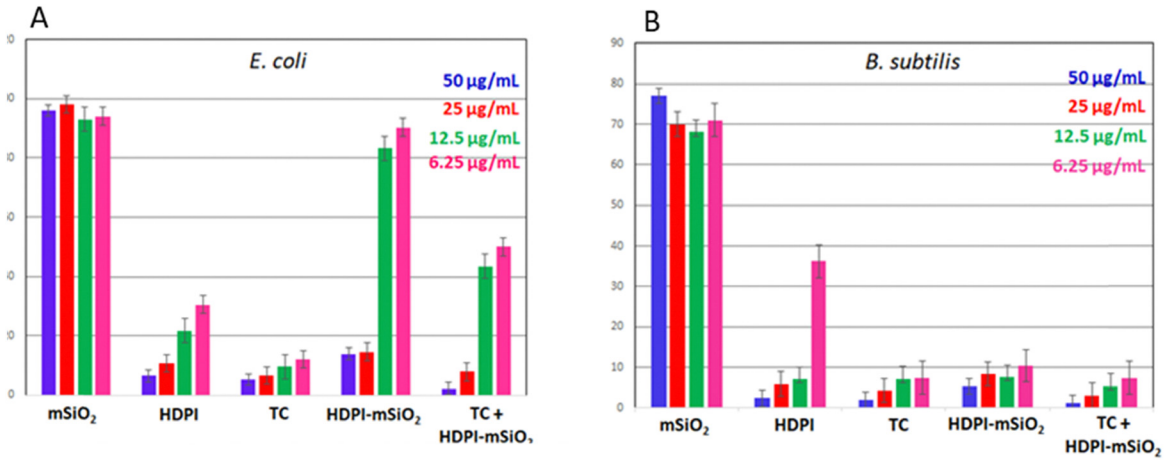

Fig. 4 Tests for the evaluation of antibacterial efficiencies of HDPI-conjugated and TC-loaded HDPI-conjugated $mSiO_2$ in different concentrations evaluated against: (A) Gram-negative bacterium *E. coli* and (B) Gram-positive bacterium *B. subtilis*. Positive control: pure HDPI and TC solutions. Negative control: bare $mSiO_2$ NPs and solvent ratio water/DMSO (10 : 1) used for the dispersion of the bare and modified $mSiO_2$, HDPI, and TC (data not shown here).

© 2025 The Author(s). Published by the Royal Society of Chemistry

Open Access Article. Published on 15 May 2025. Downloaded on 4/16/2026 5:58:42 PM.
This article is licensed under a Creative Commons Attribution 3.0 Unported Licence.

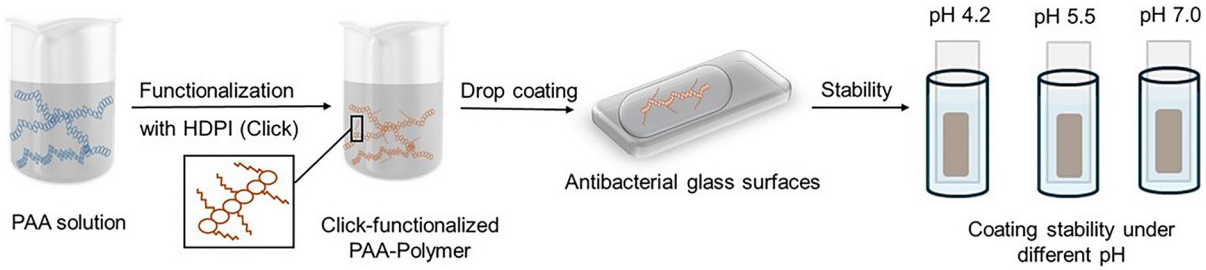

Scheme 3 Preparation of antibacterial and hydrophobic surfaces on glass substrates: Homogeneous stable hydrophobic coatings on the glass surface were produced after using the drop coating method utilizing click modified HDPI-PAA molecules. Subsequently, the coatings were evaluated for their strength under different acidic and neutral conditions in a time dependent manner up to three weeks.

1470 cm^{-1}. It is also evident that not all carboxyl groups from the PAA have reacted, as a prominent carboxyl stretching frequency at 1700 cm^{-1}, along with the C═O band at 1100 cm^{-1} is present.

The hydrophobicity of glass substrates coated with HDPI-PAA conjugates was determined by measuring the contact angle (CA) between a water droplet and the substrate (Fig. 5(B)). The HDPI-PAA sample exhibited hydrophobic behavior with a CA of 122.5°, compared to the unfunctionalized polyacrylic acid, which had a CA of 54.3° (Fig. 5(B)). The intermediates, Br-PAA and N_3-PAA, showed comparable contact angles of 83.2° and 88.8°, respectively, as expected, since bromide was substituted by an azide group in a nucleophilic substitution reaction without altering the skeleton of PAA polymer. For comparison, the contact angle of the ionic liquid on the glass was found to be 0°, confirming that HDPI imparted hydrophobicity to the glass surface.

Fig. 5(C) presents images of the coatings on glass substrates in chronological order. The stability study of the HDPI-PAA coatings on the glass surface confirmed that they remain stable for at least three weeks and resist dissolution or rupture under different acidic conditions including those simulating acidic rain (pH 4). The HDPI-PAA coated surfaces exhibited significantly higher stability against aqueous solutions probably due to the utilization (condensation) of all of the surface-attached hydroxyl groups in the functionalization step. In acidic solutions, water molecules and protons interact with fewer hydroxy groups than in pure polyacrylic acid, resulting in reduced swelling and very low solubility. This enhanced stability makes the HDPI-PAA coatings highly suitable for outdoor applications, as they can effectively withstand diverse weather conditions.

In contrast, pure PAA coatings began detaching from the glass substrate within an hour, as evident from the resulting transparent glass surface in Fig. 5(C). When exposed to a pH 4.0 solution, the PAA coating developed surface roughness within an hour. Similar roughness patterns were observed at pH 5.5 and 7.0 after 2 hours and 6 hours, respectively. At neutral pH, the solution processed slowly when compared to acidic conditions. However, after 18 days to ~3 weeks, all PAA coatings had completely dissolved under all tested pH conditions, leaving a clean glass surface.

Conclusions

Uniform mesoporous silica nanocarriers were covalently functionalized with a newly synthesized imidazolium-based long alkyl chain ionic liquid (HDPI) using a click chemistry protocol preserving its chemical structure and biological activity. These hybrid nanocarriers enable precise drug encapsulation and sustained time-dependent release of antibiotics as demonstrated with tetracycline. Toxicity assays against *E. coli* and *B. subtilis* confirmed excellent antibacterial activity, highlighting the synergistic effect of unifying HDPI and TC into a single nanocarrier. This approach underscores the potential of mesoporous nanocarriers for controlled drug delivery and stable ionic liquid-polymer surfaces, paving the way for advanced biomedical and industrial coatings.[44]

Experimental section

Synthesis of 1-hexadecyl-3-propargyl imidazolium bromide

(I) Synthesis of intermediate 1-hexadecyl imdazole (HDI). 1-Hexadecyl-3-propargyl imidazolium bromide (HDPI) was prepared using a two-step approach. Initially, 1-hexadecyl imidazole (HDI) was synthesized *via* a nucleophilic substitution reaction employing the method reported by A. Djellal and S. Amirat with several modifications under inert conditions.[28] 1.380 g (20.0 mmol) of imidazole was dissolved in 50 mL of dry dimethyl sulfoxide in a 100 mL-flask under a nitrogen atmosphere. 1.670 g of potassium hydroxide (30.0 mmol) was transferred to the flask to deprotonate the nitrogen atom of the imidazole ring, serving as a pre-activation step for the nucleophilic substitution reaction. The reaction mixture was heated up to 70 °C for 20 min. Afterwards, 6.6 mL (21.0 mmol) of 1-bromohexadecane was added dropwise within a time frame of 25 min. The reaction mixture was stirred for further 6 h at 70 °C under inert conditions. After 6 hours, the yellowish-orange reaction mixture was allowed to attain ambient temperature and 200 mL of water was added to precipitate the pale-yellow product. The precipitate was filtered and washed three times with water. The as-synthesized product was dried under reduced pressure for further characterization.

Habitus: pale-yellow powder.

Chemical formula: $C_{19}H_{36}N_2$.

Molecular weight: 292.51 g mol^{-1}.

NMR data: ^{1}H NMR (300.1 MHz, DMSO-d_6, ppm from TMS): 0.85 (3H, CH_3), 1.23 (26H, CH_2), 1.67 (2H, CH_2–C_7 chain), 3.92 (2H, N–CH_2–C_6 chain), 6.86 (1H, CH in imidazolium ring), 7.13 (1H, CH in imidazolium ring), 7.58 (1H, N–CH–N in imidazolium ring).

Open Access Article. Published on 15 May 2025. Downloaded on 4/16/2026 5:58:42 PM.
This article is licensed under a Creative Commons Attribution 3.0 Unported Licence.

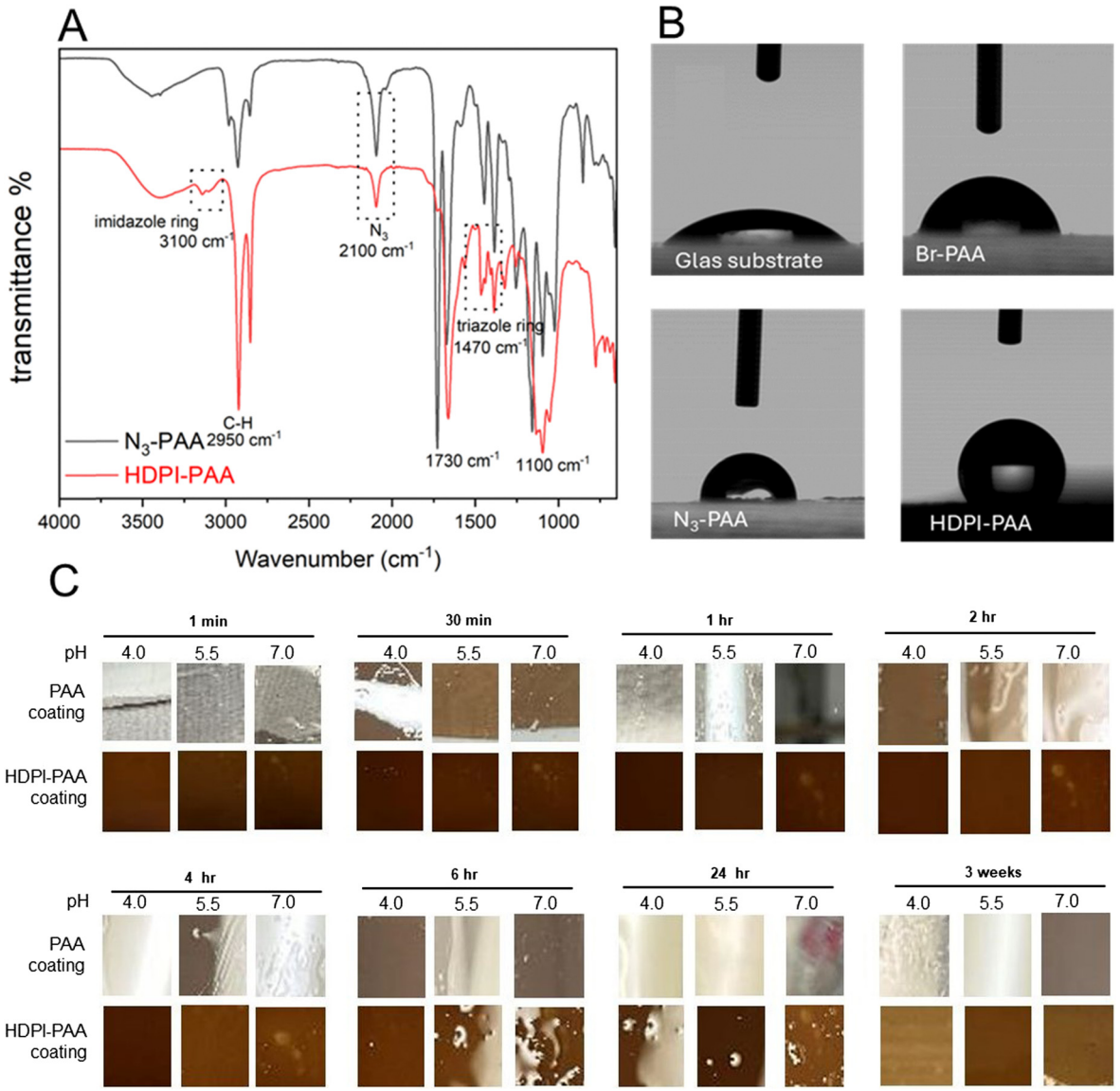

Fig. 5 (A) FT-IR spectra of polyacrylic acid before (black) and after (red) the click functionalization (B) contact angle measurements of PAA coatings at various stages of functionalization, including intermediate steps: Br-PAA 83.2°, N_3-PAA: 88.8° and clicked HDPI-PAA: 122.5°. (C) HDPI-PAA coatings (lower panel rows) on glass substrates under different pH conditions and variable time (up to 3 weeks) to determine coating stability under different environmental conditions. The upper panel rows coatings are the control samples of unfunctionalized PAA.

^{13}C NMR (DEPT(135), 75.7 MHz, DMSO-d_6, ppm from TMS): 13.93 (C_{21}), 22.09-30.57 (C_8-C_{20}). 31.29 (C_7), 45.88 (C_6), 119.14, 128.26 (C_2, C_3), 137.14 (C_5).

ESI-MS: $[M^+]$: m/z = 293.3.

(II) Synthesis of 1-hexadecyl-3-propargyl imidazolium bromide (HDPI). In the next step, 1-hexadecyl-3-propargyl imidazolium bromide (HDPI) was prepared *via* a nucleophilic substitution of 1-hexadecyl imidazole (HDI) following the experimental instruction of L. Li *et al.* with certain modifications.[28] 7.300 g (25.0 mmol) of 1-hexadecyl imidazole was dissolved in 20.0 mL of dry toluene in a 100 mL-flask. Afterwards, 2.5 mL (29.0 mmol) of propargyl bromide was added and the mixture was heated up to reflux (110 °C) for 24 h. Accordingly, the orange-brownish reaction mixture was allowed to attain ambient temperature and 100 mL of water was added to precipitate a pale-yellow product. The precipitate was filtered and washed several times with water. The as-prepared product was dried under reduced pressure for further characterization studies.

Habitus: white powder.

Chemical formula: $C_{22}H_{39}N_2Br$.

Molecular weight: 411.47 g mol^{-1}.

Yield: 74.6%.

NMR data: ^{1}H NMR (300.1 MHz, DMSO-d_6, ppm from TMS): 0.84 (3H, CH_3), 1.23 (26H, CH_2), 1.78 (2H, 2H, CH_2–C_7 chain), 3.85 (1H, CH≡C–), 4.19 (2H, N–CH_2–C_6 chain), 5.19 (2H, CH≡C–CH_2–), 7.83 (1H, CH in imidazolium ring), 7.85 (1H, CH in imidazolium ring), 9.31 (1H, N–CH–N in imidazolium ring).

^{13}C NMR (DEPT(135), 75.7 MHz, DMSO-d_6, ppm from TMS): 13.93 (C_{22}), 22.07–29.31 (C_9-C_{21}), 31.27(C_8), 49.02 (C_7), 78.98 (C_6), 122.33, 122.80 (C_2, C_3), 126.06 (C_5).

© 2025 The Author(s). Published by the Royal Society of Chemistry

Open Access Article. Published on 15 May 2025. Downloaded on 4/16/2026 5:58:42 PM. This article is licensed under a Creative Commons Attribution 3.0 Unported Licence.

ESI-MS: $[M^+]$: m/z = 330.9.

Surfactant-dependent sol–gel synthesis of mesoporous silica nanocarriers

A template-assisted sol–gel approach using cetyltrimethylammonium bromide was applied to obtain $mSiO_2$ nanocarriers following optimized protocols from Mathur *et al.*[41] Initially, 0.370 g (1.0 mmol) of cetyltrimethylammonium bromide was dissolved in 100 mL of water under magnetic stirring (700 rpm) at an elevated temperature of 80 °C followed by the addition of 0.300 g of ammonium fluoride. Afterwards, 1.78 mL of tetraethyl orthosilicate was added to the clear solution and the mixture was stirred at 700 rpm for another 1.5 hours at 80 °C. After cooling down, the white dispersion was centrifuged to collect $mSiO_2$ nanocarriers. Subsequently, nanocarriers were re-dispersed in acetone/diluted hydrochloric acid and sonicated for 30 min to ensure the extraction of any residuals of template. Finally, additional purification steps of nanocarriers with ethanol to remove any excess of released surfactant and silica were conducted. Furthermore, these particles were dried at ambient temperature for 14 hours and tested for further characterization studies.

Conjugation of 1-hexadecyl-3-propargyl imidazolium bromide onto azide-capped mesoporous silica nanocarriers

For the conjugation of 1-hexadecyl-3-propargyl imidazolium bromide onto the surface of the as-prepared $mSiO_2$ nanocarriers *via* a copper-catalyzed alkyne-azide cycloaddition, two preceding synthetic steps were required: the Br-silanization of the surface of $mSiO_2$ nanocarriers and the subsequent nucleophilic substitution of the bromide group with an azide group. Br-silanization and nucleophilic substitution of the bromide group by an azide group on the surface of $mSiO_2$ nanocarriers were conducted according to the procedure reported by Mathur *et al.*[12,30,32,36,45] Both experimental descriptions were modified to a small extent. Initially, 0.080 g of mesoporous silica nanocarriers were dispersed in 25 mL of dry toluene under an inert nitrogen atmosphere. 50 μL of 11-bromoundecyltrichlorosilane was added dropwise and the dispersion was mechanically stirred 48 hours under nitrogen at ambient temperature. After silanization, the mesoporous silica nanocarriers were separated *via* centrifugation and purified three times with ethanol to remove any excess of the residues. The resultant Br-attached mesoporous silica nanocarriers (Br-$mSiO_2$) were dried at ambient temperature for 24 hours and tested for further characterization studies. In order to provide azide groups onto the surface of $mSiO_2$ nanocarriers for the azide–alkyne click reaction, a nucleophilic substitution reaction was conducted to exchange the bromide group with an azide group. 0.080 g of Br-modified $mSiO_2$ nanocarriers (Br-$mSiO_2$) were re-dispersed in 20 mL of dry dimethyl formamide followed by the addition of 0.500 g of sodium azide. The dispersion was mechanically stirred at ambient temperature for 48 hours. Afterwards, $mSiO_2$ carriers were collected by centrifugation and purified several times with water and ethanol to remove any excess of sodium azide and by-product. After drying for 24 hours at ambient temperature, the N_3-attached mesoporous silica nanocarriers (N_3-$mSiO_2$) were prepared for further characterization studies. The CuAAC reaction was conducted to conjugate 1-hexadecyl-3-propargyl imidazolium bromide onto the surface of the as-obtained N_3-attached $mSiO_2$ nanocarriers with several modifications from the literature.[12,28,29] For this conjugation step, 0.050 g of N_3-attached $mSiO_2$ nanocarriers were dispersed in 12 mL of methanol/water (1/1). Consecutively, three solutions containing the desired ionic liquid, the copper catalyst, and a reducing agent (sodium ascorbate) were prepared separately as follows:

(1) 0.070 g of 1-hexadecyl-3-propargyl imidazolium bromide was dissolved in 5 mL of ethanol.

(2) 0.005 g of copper sulfate pentahydrate was dissolved in 2 mL of water.

(3) 0.130 g of sodium ascorbate was dissolved in 5 mL of water.

The as mentioned three solutions were added to the nanocarrier dispersion (dropwise) in the previously mentioned order (1, 2, 3). Pipetting the sodium ascorbate solution into the reaction mixture displayed a quick color change from white to a brown to bright yellow dispersion, confirming the reduction of the copper catalyst by sodium ascorbate. Furthermore, the reaction mixture was stirred at ambient temperature for 48 hours. After the reaction completed, the 1-hexadecyl imidazolium bromide-conjugated mesoporous silica nanocarriers (HDPI-$mSiO_2$) were collected *via* centrifugation and purified with ethanol (5 × 5000 rpm, 10 min) to remove any reactants and/or unbound moieties. Drying at ambient temperature for 24 hours provided 1-hexadecyl-3-propargyl imidazolium bromide-conjugated mesoporous silica nanocarriers for further characterization and development of drug delivery carriers.

Drug release studies of tetracycline-loaded 1-hexadecyl-3-propargyl-conjugated mesoporous silica nanocarriers

To investigate the time-dependent release profiles of tetracycline-loaded 1-hexadecyl-3-propargyl imidazolium bromide-conjugated $mSiO_2$ nanocarriers (TC + HDPI-$mSiO_2$) in comparison to bare tetracycline-loaded $mSiO_2$ nanocarriers (TC + $mSiO_2$), continuous release studies with tetracycline (TC) were conducted. For these studies, 15 mg of nanocarriers were loaded with tetracycline by dispersing and stirring them in 15 mL of a tetracycline stock solution (c = 0.1128 mg of tetracycline per mL ethanol) overnight in the dark. Afterwards, nanocarriers were separated from the solution *via* centrifugation and the loading capacity of the nanocarriers was determined by measuring the concentration of tetracycline in the collected supernatants *via* UV-vis spectroscopy based on the difference from the stock solution (absorption maximum tetracycline: λ_{max} = 270 nm). In the meantime, tetracycline-loaded nanocarriers were dispersed in 6 mL of PBS (pH 7.4) and stirred at 400 rpm at a temperature of 37 °C in the dark. After some pre-determined time-intervals (1, 2, 3, 4, 24, and 48 hours), nanocarriers were separated again from the solution *via* centrifugation and 2 mL of the supernatant was applied in UV-vis analysis to determine the released amount of tetracycline from the nanocarriers. Then, the supernatant was added back again

Open Access Article. Published on 15 May 2025. Downloaded on 4/16/2026 5:58:42 PM. This article is licensed under a Creative Commons Attribution 3.0 Unported Licence.

(continuous release studies). This procedure was repeated for the preassigned points in time.

Synthesis of HDPI-functionalized polyacrylic acid

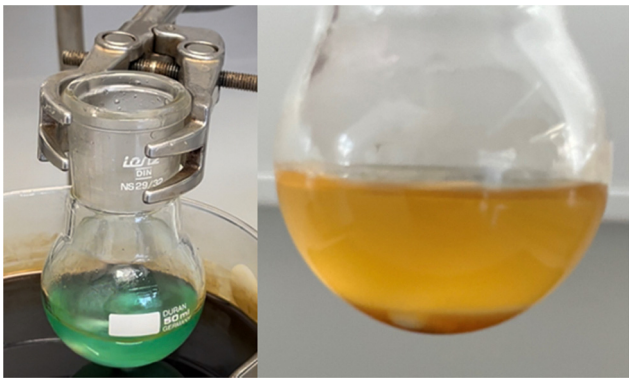

Polyacrylic acid (230 mg) and (11-bromoundecyl)trichlorosilane (500 μl) were stirred in ethanol (20 mL) at 50 °C and 300 rpm for 24 hours. The ethanol was evaporated, and the residue was taken up in DMF (10 mL) and treated with sodium azide (200 mg, green solution) and stirred at 60 °C and 350 rpm for 48 hours. Subsequently, the ionic liquid was prepared for the click reaction. Copper sulfate (140 mg) in H_2O (2 mL), HDPI (400 mg) in ethanol (2 mL), and sodium ascorbate (750 mg) in H_2O (2 mL) were combined, stirred for 20 minutes, and then slowly added dropwise to the reaction mixture (brownish solution). After 50 hours/3 days at 55 °C and 350 rpm, the product was purified with water and separated by centrifugation (5000 rpm, 20 min).[12] The brown solid product was dried under reduced pressure for 16 hours.

Stability study of HDPI-functionalized polyacrylic acid

The HDPI-modified polymer was dissolved in THF and applied to a clean glass substrate using a drop-casting method. The resulting polymeric films were then dried at ambient temperature for 2 hours before being immersed in aqueous solutions. To assess the stability of polymeric coatings under various acidic conditions, the coated glass substrates were exposed to solutions with pH values of 4.0, 5.5, and 7 for a total duration of 432 hours. The coatings were tested at pH 4.0, pH 5.5, and pH 7.0 for 432 hours. At regular intervals, the glass substrates were removed from their solutions and photographed to observe any changes. For comparison, the same procedure was conducted using unmodified PAA as reference samples.

In vitro antibacterial testing: *p*-iodonitrotetrazolium-chloride/(INT) violet assay

To evaluate the antimicrobial activity of certain bare and modified silica nanocarriers against Gram-positive and Gram-negative bacteria, two iodonitrotetrazolium-chloride (INT) violet assays (colorimetric viability assay) were carried out for the hereinafter referred nanoaggregates and nanocarriers ($mSiO_2$, HDPI-$mSiO_2$, TC + HDPI-$mSiO_2$).[12] This method is used for the confirmation of the viability of bacteria cells in proliferation and it is based on a tetrazolium-based reagent called INT, which is converted *via* reduction to a violet formazan dye in the presence of metabolically active bacteria. Therefore, model bacteria *E. coli* and *B. subtilis* were cultured in *Mueller Hinton*-broth overnight at 37 °C while mild shaking (180 rpm). Overnight-cultured bacteria were added to a fresh medium and grown to an optical density of 0.7 at 600 nm. Each 10 μL of bacterial solution was added in triplicate to wells of a 96-well plate (*BD Falcon*, USA). The previously mentioned nanoaggregates and nanocarriers were used at variable concentrations (0.00625 mg mL^{-1}, 0.01250 mg mL^{-1}, 0.02500 mg mL^{-1} and 0.05000 mg mL^{-1}) dispersed in water/dimethyl sulfoxide (10 : 1) and 180 μL of *Mueller Hinton*-medium were added to each corresponding well and incubated for 6 h at 37 °C. Water/dimethyl sulfoxide (10 : 1) and bare magnetic nanoaggregates and mesoporous silica nanocarriers were used as negative controls, and a solution of pure antibiotic (1-hexadecyl-3-propargyl imidazolium bromide/tetracycline) was dissolved in water/dimethyl sulfoxide (10 : 1) as a positive control. After the incubation time, 10 μL of the freshly prepared *p*-iodonitrotetrazolium-chloride solution (1 mg mL^{-1} in dimethyl sulfoxide) was added to each well and incubated for further 30 min at 37 °C. The viability of bacteria relative to the untreated control was determined by measuring the absorption at 540 nm on a *Tecan infinite M200* plate reader.

Data availability

The data supporting the findings of this study, Ionic Liquid Modified Mesoporous Silica Nanocarriers for Efficient Drug Delivery and Hydrophobic Surface Engineering, are available within the article and its ESI.† All relevant data, including the synthesis procedures, characterization details, and experimental results related to the modification of mesoporous silica nanocarriers with ionic liquids for drug delivery and hydrophobic surface engineering and applications are provided. Additional data (*e.g.*, raw experimental data, detailed spectral analysis, or other ESI†) can be accessed upon reasonable request from the corresponding author.

Conflicts of interest

The authors declare that there are no conflicts of interest regarding the publication of this manuscript. All authors have reviewed and approved the final version of the manuscript.

Acknowledgements

Authors would like to acknowledge the University of Cologne (UoC) for the infrastructural and financial support through the Transformative Nanocarriers for RNA Transport and Tracking – Advanced Concepts for Therapy and Diagnostic. We also thank Dr. T. Fischer (UoC) for TEM measurements and Prof. I. Neundorf (UoC) and Dr. M. Drexelius for their support for antibacterial testing of the mesoporous silica nanocarriers.

© 2025 The Author(s). Published by the Royal Society of Chemistry

Open Access Article. Published on 15 May 2025. Downloaded on 4/16/2026 5:58:42 PM. This article is licensed under a Creative Commons Attribution 3.0 Unported Licence.

References

1 (*a*) R. Vivas, A. A. T. Barbosa, S. S. Dolabela and S. Jain, Multidrug-Resistant Bacteria and Alternative Methods to Control Them: An Overview, *Microb. Drug Resist.*, 2019, **25**(6), 890–908; (*b*) M. Zare, K. Namratha, S. Ilyas, A. Sultana, A. Hezam, M. A. Surmeneva, M. B. Nayan, S. Ramakrishna, S. Mathur and K. Byrappa, Emerging trends for ZnO nanoparticles and their applications in food packaging, *ACS Food Sci. Technol.*, 2022, **2**(5), 763–781.

2 J. Guan, Y. Wang, S. Wu, Y. Li and J. Li, Durable Anti-Superbug Polymers: Covalent Bonding of Ionic Liquid onto the Polymer Chains, *Biomacromolecules*, 2017, **18**(12), 4364–4372.

3 M. Hong, M. Hong, Z. Miao, Z. Miao, X. Xu, X. Xu, Q. Zhang and Q. Zhang, Magnetic Iron Oxide Nanoparticles Immobilized with Sugar-Containing Poly(Ionic Liquid) Brushes for Efficient Trapping and Killing of Bacteria, *ACS Appl. Bio Mater.*, 2020, **3**(6), 3664–3672.

4 B. Yoo, Y. Zhu and E. J. Maginn, Molecular Mechanism of Ionic-Liquid-Induced Membrane Disruption: Morphological Changes to Bilayers, Multilayers, and Vesicles, *Langmuir*, 2016, **32**(21), 5403–5411.

5 D. Wang, D. H. De Jong, A. Rühling, V. Lesch, K. Shimizu, S. Wulff, A. Heuer, F. Glorius and H. J. Galla, Imidazolium-Based Lipid Analogues and Their Interaction with Phosphatidylcholine Membranes, *Langmuir*, 2016, **32**(48), 12579–12592.

6 M. C. Jennings, K. P. C. Minbiole and W. M. Wuest, Quaternary Ammonium Compounds: An Antimicrobial Mainstay and Platform for Innovation to Address Bacterial Resistance, *ACS Infect. Dis.*, 2016, **1**(7), 288–303.

7 N. Raheem and S. K. Straus, Mechanisms of Action for Antimicrobial Peptides With Antibacterial and Antibiofilm Functions, *Front. Microbiol.*, 2019, **10**, 1–14.

8 F. Nederberg, Y. Zhang, J. P. K. Tan, K. Xu, H. Wang, C. Yang, S. Gao, X. D. Guo, K. Fukushima and L. Li, *et al.*, Biodegradable Nanostructures with Selective Lysis of Microbial Membranes, *Nat. Chem.*, 2011, **3**, 409–414.

9 G. S. Lim, J. Zidar, D. W. Cheong, S. Jaenicke and M. Klähn, Impact of Ionic Liquids in Aqueous Solution on Bacterial Plasma Membranes Studied with Molecular Dynamics Simulations, *J. Phys. Chem. B*, 2014, **118**, 10444–10459.

10 J. Łuczak, C. Jungnickel, I. Łącka, S. Stolte and J. Hupka, Antimicrobial and Surface Activity of 1-Alkyl-3-Methylimidazolium Derivatives, *Green Chem.*, 2010, **12**, 593–601.

11 L. Carson, P. K. W. Chau, M. J. Earle, M. A. Gilea, B. F. Gilmore, S. P. Gorman, T. Mccann and K. R. Seddon, Antibiofilm Activities of 1-Alkyl-3-Methylimidazolium Chloride Ionic Liquids, *Green Chem.*, 2009, **11**, 492–497.

12 A. Szymura, S. Ilyas, M. Horn, I. Neundorf and S. Mathur, Multivalent Magnetic Nanoaggregates with Unified Antibacterial Activity and Selective Uptake of Heavy Metals and Organic Pollutants, *J. Mol. Liq.*, 2020, **317**(114002), 1–11.

13 N. Nikfarjam, M. Ghomi, T. Agarwal, M. Hassanpour, E. Sharifi, D. Khorsandi, M. A. Khan, F. Rossi, A. Rossetti and E. N. Zare, *et al.*, Antimicrobial Ionic Liquid-Based Materials for Biomedical Applications, *Adv. Funct. Mater.*, 2021, **31**(42), 1–27.

14 B. Jing, N. Lan, J. Qiu and Y. Zhu, Interaction of Ionic Liquids with a Lipid Bilayer: A Biophysical Study of Ionic Liquid Cytotoxicity, *J. Phys. Chem. B*, 2016, **120**(10), 2781–2789.

15 C. Zhou, F. Wang, H. Chen, M. Li, F. Qiao, Z. Liu, Y. Hou, C. Wu, Y. Fan and L. Liu, *et al.*, Selective Antimicrobial Activities and Action Mechanism of Micelles Self-Assembled by Cationic Oligomeric Surfactants, *ACS Appl. Mater. Interfaces*, 2016, **8**, 4242–4249.

16 A. Shaheen, R. Arif, A. W. Mir and S. Rehman, Synthesis, Physicochemical Characteristics and Antimicrobial Studies of Ethyl-Substituted Imidazolium-Based Surface Active Ionic Liquids (SAILs), *Colloids Interface Sci. Commun.*, 2019, **33**, 100204.

17 M. T. Garcia, I. Ribosa, L. Perez, A. Manresa and F. Comelles, Aggregation Behavior and Antimicrobial Activity of Ester-Functionalized Imidazolium- and Pyridinium-Based Ionic Liquids in Aqueous Solution, *Langmuir*, 2013, **29**(8), 2536–2545.

18 Z. Gounani, M. A. Asadollahi, J. N. Pedersen, J. Lyngsø, J. S. Pedersen, A. Arpanaei and R. L. Meyer, Mesoporous Silica Nanoparticles Carrying Multiple Antibiotics Provide Enhanced Synergistic Effect and Improved Biocompatibility, *Colloids Surf., B*, 2019, **175**, 498–508.

19 M. Marimani, Combination Therapy against Multidrug Resistance, in *Combination Therapy Against Multidrug Resistance*, ed. M. Y. Wani and A. Ahmad, Academic Press, Elsevier Inc., 2020, pp. 39–64.

20 H. Deng, D. McShan, Y. Zhang, S. S. Sinha, Z. Arslan, P. C. Ray and H. Yu, Mechanistic Study of the Synergistic Antibacterial Activity of Combined Silver Nanoparticles and Common Antibiotics, *Environ. Sci. Technol.*, 2016, **50**, 8840–8848.

21 B. F. Gilmore, G. P. Andrews, G. Borberly, M. J. Earle, M. A. Gilea, S. P. Gorman, A. F. Lowry, M. McLaughlin and K. R. Seddon, Enhanced Antimicrobial Activities of 1-Alkyl-3-Methyl Imidazolium Ionic Liquids Based on Silver or Copper Containing Anions, *New J. Chem.*, 2013, **37**, 873–876.

22 Z. Zheng, J. Guo, H. Mao, Q. Xu, J. Qin and F. Yan, Metal-Containing Poly(Ionic Liquid) Membranes for Antibacterial Applications, *ACS Biomater. Sci. Eng.*, 2017, **3**(6), 922–928.

23 O. Lebedeva, D. Kultin and L. Kustov, Advanced research and prospects on polymer ionic liquids: trends, potential and application, *Green Chem.*, 2023, **25**(22), 9001–9019.

24 L. Xiao, M. Mertens, L. Wortmann, S. Kremer, M. Valldor, T. Lammers, F. Kiessling and S. Mathur, *ACS Appl. Mater. Interfaces*, 2015, **7**(12), 6530–6540.

25 R. Ferraz, D. Silva, A. R. Dias, V. Dias, M. M. Santos, L. Pinheiro, C. Prudêncio, J. P. Noronha, Ž. Petrovski and L. C. Branco, Synthesis and Antibacterial Activity of Ionic Liquids and Organic Salts Based on Penicillin g and Amoxicillin Hydrolysate Derivatives against Resistant Bacteria, *Pharmaceutics*, 2020, **12**(221), 1–23.

Open Access Article. Published on 15 May 2025. Downloaded on 4/16/2026 5:58:42 PM. This article is licensed under a Creative Commons Attribution 3.0 Unported Licence.

26 K. S. Egorova, E. G. Gordeev and V. P. Ananikov, Biological Activity of Ionic Liquids and Their Application in Pharmaceutics and Medicine, *Chem. Rev.*, 2017, **117**, 7132–7189.
27 M. Colonna, C. Berti, E. Binassi, M. Fiorini, S. Sullalti, F. Acquasanta, M. Vannini, D. Di Gioia and I. Aloisio, Imidazolium Poly(Butylene Terephthalate) Ionomers with Long-Term Antimicrobial Activity, *Polymer*, 2012, **53**, 1823–1830.
28 A. Djellal and S. Amirat, Synthesis of Some Functionalized Ionic Liquids with Long Chain of Carbone Starting from Imidazole, *Orient. J. Chem.*, 2015, **31**, 2391–2394.
29 L. Li, J. Wang, T. Wu and R. Wang, Click Ionic Liquids: A Family of Promising Tunable Solvents and Application in Suzuki-Miyaura Cross-Coupling, *Chem. – Eur. J.*, 2012, **18**(25), 7842–7851.
30 A. M. Renner, S. Ilyas, H. A. Schlößer, A. Szymura, S. Roitsch, K. Wennhold and S. Mathur, Receptor-Mediated in Vivo Targeting of Breast Cancer Cells with 17α-Ethynylestradiol-Conjugated Silica-Coated Gold Nanoparticles, *Langmuir*, 2020, **36**, 14819–14828.
31 M. I. Hutchings, A. W. Truman and B. Wilkinson, Antibiotics: Past, Present and Future, *Curr. Opin. Microbiol.*, 2019, **51**, 72–80.
32 S. Ilyas, N. K. Ullah, M. Ilyas, K. Wennhold, M. Iqbal, H. A. Schlößer, M. S. Hussain and S. Mathur, Mediating the Fate of Cancer Cell Uptake: Dual-Targeted Magnetic Nanovectors with Biotin and Folate Surface Ligands, *ACS Biomater. Sci. Eng.*, 2020, **6**, 6138–6147.
33 K. Raiah, A. Djalab, A. Hadj-Ziane-Zafour, B. Soula, A. M. Galibert and E. Flahaut, Influence of the Hydrocarbon Chain Length of Imidazolium-Based Ionic Liquid on the Dispersion and Stabilization of Double-Walled Carbon Nanotubes in Water, *Colloids Surf., A*, 2015, **469**, 107–116.
34 N. Z. Fantoni, A. H. El-Sagheer and T. Brown, A hitchhiker's guide to click-chemistry with nucleic acids, *Chem. Rev.*, 2021, **121**(12), 7122–7154.
35 M. B. Schütz, K. Lê, S. Ilyas and S. Mathur, Reversible Covalent Assembly of Nanoparticles through On-Surface Diels-Alder Reaction, *Langmuir*, 2020, **36**(6), 1552–1558.
36 M. B. Schütz, S. Ilyas, K. Lê, M. Valldor and S. Mathur, Nanoparticle Arrays Having Directed Hybrid Topology via Covalent Self-Assembly of Iron Oxide and Silica Nanoparticles, *ACS Appl. Nano Mater.*, 2020, **3**(6), 5936–5943.
37 G. Y. Wang, Y. Y. Wang and X. H. Wang, Aggregation Behaviors of Mixed Systems for Imidazole Ionic Liquid Surfactant and Triton X-100, *J. Mol. Liq.*, 2017, **232**, 55–61.
38 M. B. Schütz, A. M. Renner, S. Ilyas, K. Lê, M. Guliyev, P. Krapf, B. Neumaier and S. Mathur, 18F-Labeled Magnetic Nanovectors for Bimodal Cellular Imaging, *Biomater. Sci.*, 2021, **9**, 4717–4727.
39 M. Kim, D. Ki, Y. Na, H. Lee, J. Baek, J. Lee, H. Lee and C. Cho, Optimization of Mesoporous Silica Nanoparticles through Statistical Design of Experiment and the Application for the Anticancer Drug, *Pharmaceutics*, 2021, **13**(184), 1–18.
40 S. Iqbal, T. J. K. Schneider, T. T. Truong, R. Ulrich-Müller, P. H. Nguyen, S. Ilyas and S. Mathur, Carriers for hydrophobic drug molecules: lipid-coated hollow mesoporous silica particles, and the influence of shape and size on encapsulation efficiency, *Nanoscale*, 2024, **16**(23), 11274–11289.
41 S. llyas, S. E. M. Sahnoun, A. Szymura, J. Pes, S. Habib, A. Florea, L. Schäfer, E. M. Buhl, A. Morgenroth, P. Habib, F. M. Mottaghy and S. Mathur, Validation of Dual-Action Chemo-Radio-Labeled Nanocarriers with High Efficacy against Triple-Negative Breast Cancer, *ACS Appl. Mater. Interfaces*, 2023, **15**(42), 48963–48977.
42 C. Maton, N. De Vos and C. V. Stevens, Ionic Liquid Thermal Stabilities: Decomposition Mechanisms and Analysis Tools, *Chem. Soc. Rev.*, 2013, **42**(13), 5963–5977.
43 H. Yasin, B. Al-Taani and M. Salem, Preparation of Ethylcellulose Microspheres for Sustained-Release of Pregabalin, *Res. Pharm. Sci.*, 2021, **16**(1), 1–15.
44 (*a*) M. Maleki, M. Amani-Tehran, M. Latifi and S. Mathur, Computer Drug Release Profile in Core–Shell Nanofibrous Structures: A Study on Peppas Equation and Artificial Neural Network Modeling, *Comput. Methods Programs Biomed.*, 2014, **113**(1), 92–100; (*b*) E. Y. Chen, W. F. Liu, L. Megido, P. Díez, M. Fuentes, C. Fager, E. Olsson, I. Gessner and S. Mathur, Understanding and Utilizing the Biomolecule/Nanosystems Interface, *Nanotechnol. Prev. Regener. Med.*, 2018, 207–297; (*c*) S. Iqbal; S. Ilyas and S. Mathur, Solid Nanocarriers and Bioconjugation Strategies for Efficient *In Vivo* Drug Transport, in *Characterisation of Drug Nanocarriers*, ed. I. Vinković Vrček, J. M. de la Fuente, V. Uskoković, Royal Society of Chemistry, 2024, pp. 34–72.
45 S. Ilyas, M. Ilyas, R. A. van der Hoorn and S. Mathur, Selective conjugation of proteins by mining active proteomes through click-functionalized magnetic nanoparticles, *ACS Nano*, 2013, **7**(11), 9655–9663.

© 2025 The Author(s). Published by the Royal Society of Chemistry